Plasmonics (2013) 8:361–368
DOI 10.1007/s11468-012-9398-5

Surface Plasmon Coupled Whispering Gallery Mode for Guided and Free-Space Electromagnetic Waves

Manas Ranjan Gartia · Meng Lu · Gang Logan Liu

Received: 9 January 2012 / Accepted: 28 May 2012 / Published online: 16 June 2012

Abstract We demonstrate theoretically that plane wave propagating in free space can be used to excite the whispering gallery mode in dielectric microresonators grown on the top of nanoplasmonic structures, with the assistance of surface plasmon wave. We have demonstrated the coupling modes using both localized and propagating surface plasmon-supporting nanostructure surfaces.

Keywords Whispering gallery mode · Surface plasmon

Introduction

Optical whispering gallery mode (WGM) resonators in the form of microring, microdisk, microtoroid, micropillar, and microsphere have been demonstrated in recent years [1]. The potential applications include various photonic applications such as label-free biosensing [2], microlasers [3], narrow filters optical switching [4], as well as for fundamental studies such as nonlinear optics [5], quantum optics (quantum electrodynamics, Purcell enhancement, emitter–photon coupling) [6–8], and quantum communication [9]. It is well known that dielectric sphere structure can sustain high-Q electromagnetic WGM with Q-factor as high as 10^{11} (and hence resonance line width, kilohertz; decay time, microsecond; and decay length, kilometer) as compared to typical rings, disk Q-factor of $10^{3–5}$ (resonance line width, gigahertz; decay time, picosecond; and decay length, millimeter) and that of microtoroid Q-factor of 10^8 (resonance line width, megahertz; decay time, nanosecond; and decay length, meter) [1]. Though, microsphere offer tight confinement and high enhancement of optical field, however, coupling of light into the microsphere is a difficult task due to weak exponentially decaying evanescent external fields [10]. Since, it requires precise overlapping of the evanescent field of WGM waves with the evanescent field of the phase matched optical waveguides, it has been demonstrated only with precise positioned optical elements such as optical fiber (tapered, etch eroded, side polished, half-block fiber coupler), planar waveguides, or prisms [11]. These methods require tight control and precision on fabrication as well as alignment in the optical near field. In addition, due to quasi-degeneracy of these modes and lack of miniaturization (in order to achieve minimal reflection loss due to curvature) high-Q WGM has restricted application in biotechnology which demands multiplexing and simplicity of use [10].

Recently, efficient coupling of propagating fiber modes [12] and of radiative fields of dipole emitters [13] into whispering gallery (WG) modes has been demonstrated in dielectric microspheres with the aid of surface plasmon modes of noble metal nanoparticles. However, an analytical model for the theory of coupling is clearly missing in their description and the demonstration is restricted only to localized surface plasmon (SP) modes. Here, we demonstrate easy coupling between the microresonators and free-space

Electronic supplementary material The online version of this article (doi:10.1007/s11468-012-9398-5) contains supplementary material, which is available to authorized users.

M. R. Gartia
Department of Nuclear, Plasma and Radiological Engineering,
University of Illinois,
Urbana, IL, USA

M. Lu · G. L. Liu
Department of Electrical and Computer Engineering,
University of Illinois,
Urbana, IL, USA

M. R. Gartia · M. Lu · G. L. Liu (✉)
Micro and Nanotechnology Laboratory, University of Illinois,
Urbana, IL 61801, USA
e-mail: loganliu@illinois.edu

wave for frequencies in the vicinity of the surface plasmon resonance using both localized SP (such as noble-metal nanoparticles) and propagating SP modes (such as grating like structures). In this mechanism, the nanostructure can act as dielectric scatterer and thereby decomposing the incoming wave in to discrete set of spherical (or cylindrical) modes. Some of these modes can be coupled to the WG modes of dielectric microresonators. Similar formalism for scattering particle [14] and corrugated grating structure [15] for exchange of modes has been proposed using coupled mode theory. A model, as given below, is provided to describe the coupling of SP waves into WG modes. Finally, finite element method-based commercial software, COMSOL, has been used to obtain WG modes for spherical microresonator grown on the top of SP supporting substrates.

Theoretical Model for the Coupling

The whispering gallery modes are generally described by Maxwell vector wave equation, which reduces to Helmholtz equation for a homogeneous material with azimuthal symmetry [16] as:

$$\nabla^2 \psi_{l,m,n}(r,\theta,\phi) + k^2 \psi_{l,m,n}(r,\theta,\phi) = 0 \tag{1}$$

where $k = k_0(\varepsilon\mu)^{1/2}$ and $k_0 = \omega/c$. The field can be found using the separation of variable technique as $\psi_{l,m,n}(r,\theta,\phi) = N_s\,\psi_r(r)\psi_\theta(\theta)\psi_\phi(\phi)$ where r, θ, and ϕ describe the radial, polar and azimuthal direction of field respectively and N_s is the normalizing coefficient derived in reference [11]. Whispering gallery modes are characterized as three mode numbers (n, m, l) which are the radial, azimuthal (or equatorial) and angular (or polar) mode numbers, respectively. The radial part of a sphere WGM can be described by spherical Bessel functions with an external evanescent tail, while the polar (longitudinal) field dependence follows spherical harmonics, and the equatorial (azimuthal or latitudinal) field variation is sinusoidal [11]. Finally, the integration strength between two interacting modes can be described by using coupled mode theory with writing the overlap integral. For example, the coupling between fiber mode and a perfect dielectric sphere can be written as [11]:

$$\kappa = \frac{k^2}{2\beta_f} \int_x \int_y \left(n_s^2 - n_0^2\right) F_0\, \psi_{l,m,n}\, dx\, dy \tag{2}$$

where n_s, n_0 are the refractive index of sphere and surrounding medium respectively. It should be noted that Eq. (2) is valid only for small refractive index contrast. Here, F_0 describes the field of an optical fiber, the analytical solution for which is well known [11]. F_0 is generally a Bessel function of zeroth and first order assuming linearly polarized fields and taking in to consideration the radial dependence of the fundamental mode. So F_0 will be a function of r. To carry out the integration, transformation of polar coordinates to Cartesian coordinates needs to be performed. For the coupling between surface plasmon mode and WGM, we have to find an expression similar to F_0 in order to write the overlap integral, which generally describe the rate of increase in amplitude of the sphere mode (and hence for fiber coupled WGM, κ^2 is the amount of power coupled out of the fiber into the sphere per revolution) [11].

It should be noted that both the modes: the one in planar waveguide and that in surface plasmons are guided modes. The waveguide modes are guided by the total internal reflection in the waveguide film and the surface plasmon modes are guided by the metal dielectric interface [17]. However, the strength of the evanescent field for surface plasmon is larger than that for waveguide modes (due to field enhancement near surface plasmon resonance) [18]. Therefore, in comparison to waveguide modes, the sensitivity is typically larger with surface plasmon resonances [18]. In fact, a combination of surface plasmons and waveguide modes is possible [18]. It is well known that the surface plasmons are transverse magnetic (TM) or p-polarized electromagnetic waves that propagate along the interface between a metal film and a dielectric medium. The mth order surface plasmon (where m=0, 1, 2… is the mode number) propagating in the x-direction can be described by the y-component of its magnetic field as [17] $H_y(x,t) = v_m(x,t) = v_m(z)\exp[i(k_x x - \omega t)]$ where $v_m(x,\ t)$ is the scalar field function, $v_m(z)$ is the transverse field distribution of the mode and k_x is the propagation constant. Similarly, the localized surface plasmon resonance (LSPR) mode of a spherical nanostructure with radius "a" excited by a z-polarized light of wavelength λ (with a/λ<0.1) is given by [19]: $E \times (x,y,z) = E_0\hat{\mathbf{z}} - \left[\frac{\varepsilon_M-\varepsilon_D}{\varepsilon_M+2\varepsilon_D}\right] a^3 E_0 \left[\frac{\hat{\mathbf{z}}}{r^3} - \frac{3z}{r^5}\left(x\hat{\mathbf{x}} + y\hat{\mathbf{y}} + z\hat{\mathbf{z}}\right)\right]$. The field of surface plasmon in the dielectric medium is an evanescent wave and is given by $v_m(z) = v_m(0)\exp(-z/\Delta z_D)$ where $\Delta z_D = (\lambda/2\pi)\left[n^2 - n_D^2\right]^{-\frac{1}{2}}$ is the penetration depth. Here, n is the effective refractive index of the surface plasmon wave given by $n = k_x/k_0 = \left[(n_D)^{-2} + (\varepsilon_M)^{-1}\right]^{-\frac{1}{2}}$. The penetration depth in terms of effective refractive index can be written as $\Delta z_D = (\lambda/2\pi n_D n)[-\varepsilon_M]^{\frac{1}{2}}$. It should also be noted that the surface plasmon field in the metal also decays exponentially with increasing distance from the interface and the penetration depth is given by $\Delta z_M = \Delta z_D n_D^2/(-\varepsilon_M)$. Here the subscript D is used for dielectric and M is used for metal. The metal is assumed to have a complex dielectric function $\varepsilon_M = \varepsilon_M^{'} + i\varepsilon_M^{''}$ and the real part is negative. Now the coupling mode between surface plasmon (SP) and dielectric WGM can be written by replacing the overlapping integral

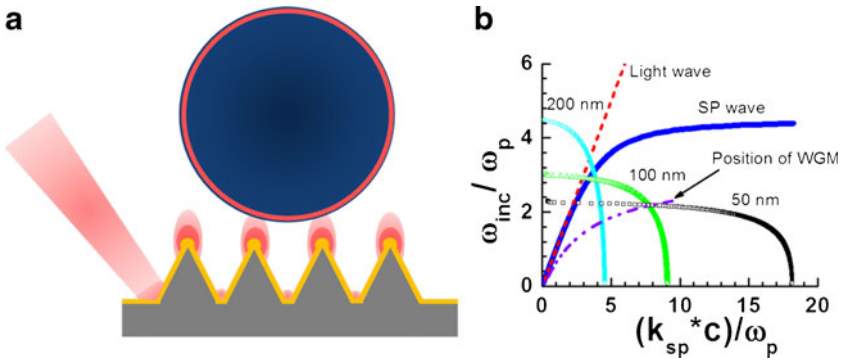

Fig. 1 **a** Schematic of the coupling scheme for surface plasmon generated by free-space electromagnetic waves and a dielectric microresonator. **b** Overlay of dispersion curve for light wave, WGM and SP wave, and the resonance modes spectra for periodic plasmonic grating with 50, 100, and 200 nm periodicities

by the expression $F_0 = N_{sp}\exp(-z/\Delta z_D)$ *if* $z > 0$ and $F_0 = N_{sp}\exp(-z/\Delta z_M)$ *if* $z < 0$, where N_{sp} describe the transverse field distribution for surface plasmon with mode number m.

Results and Discussion

A schematic of the proposed scheme for plasmonic coupled WGM is shown in Fig. 1a. The near field produced by the plane wave excitation on a grating structure or random surface roughness can excite SPs. Figure 1b shows the dispersion curve for a SP mode on a smooth surface and for a periodic hole grating structure (as analytical expression is available for subwavelength holes structure [20]). In the same plot, we have also shown the frequency-dependent WGM mode position (analytical expression taken from [21]). The permittivity of the metal (silver) is modeled by the Drude model with a plasma frequency of $\omega_p = 1.32 \times 10^{16} s^{-1}$ $(or\ 8.6\,eV)$ and a relaxation time of $\tau = 1.45 \times 10^{-14} s$ (or damping coefficient $\gamma = 0.045\,eV$) [22]. This figure clearly showed the existence of coupling mode between WGM and SP mode from grating-like structure. Further, in order to couple SP mode into microresonator, there should be available modes in the microresonators for the frequencies in the vicinity of the SP resonance. The supporting modes for a 2 μm silica sphere are analyzed by Modal analysis using COMSOL. The structure has (n=1, m=5) and (n=2, m=3) resonance mode for frequencies 526 and 585 THz, respectively, as shown in Fig. 2a and b. After coating the sphere with 80 nm silver, the modal analysis shows the (n=1, m=8) resonance mode for the dielectric, due to coupling to surface plasmon resonance (SPR; Fig. 2d) near the frequency of 556 THz (540 nm). A second-order resonance mode (n=2, m=2) inside the dielectric also showed up (Fig. 2c) at frequency of 551 THz, which did not show any SP coupling behavior.

Figure 3a shows a SEM image of nanophotonic structure fabricated on silicon using ICP-RIE processing. The details of the fabrication process are given in [23, 24]. The height of the nanocone structures are about 200 nm, the base of the cones are 120 nm and the distance between two cone structures is about 300 nm. SEM of the nanoplasmonic structure after deposition of 80 nm silver on the nanophotonic structure is shown in Fig. 3b. The presence of SPR in our fabricated nanoplasmonic structure is independently verified by using two commercially available electromagnetic simulation packages (DIFFRACTMOD, RSoft Design, and COMSOL). DIFFRACTMOD uses rigorous coupled-wave analysis (RCWA) and can provide information about diffraction efficiency as a function of wavelength. The absorption maxima (or reflection minima) of the calculated spectra can be utilized to identify the resonant mode. For the RCWA simulation, we used a silicon cone structure with height 200 nm, base 120 nm, with a period of 300 nm. The thickness of silver layer on the top of the silicon cones are

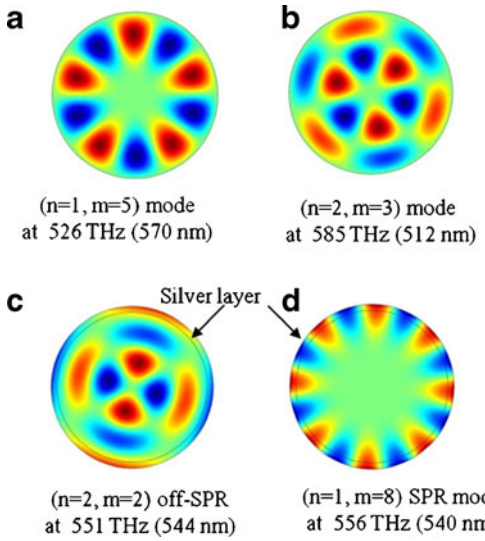

Fig. 2 Modal analysis of silica microresonator with refractive index of 1.59 and diameter 2 μm. **a** (n=1, m=5) WG mode of the microresonator at resonance frequency 526 THz. **b** (n=2, m=3) WG mode the microresonator at resonance frequency 585 THz. Modal analysis showing the resonance after coating 80 nm silver on the silica microresonator. **c** (n=2, m=2) Off-surface plasmon coupled WG mode at 551 THz. **d** (n=1, m=8) Surface plasmon-coupled WG mode at 556 THz

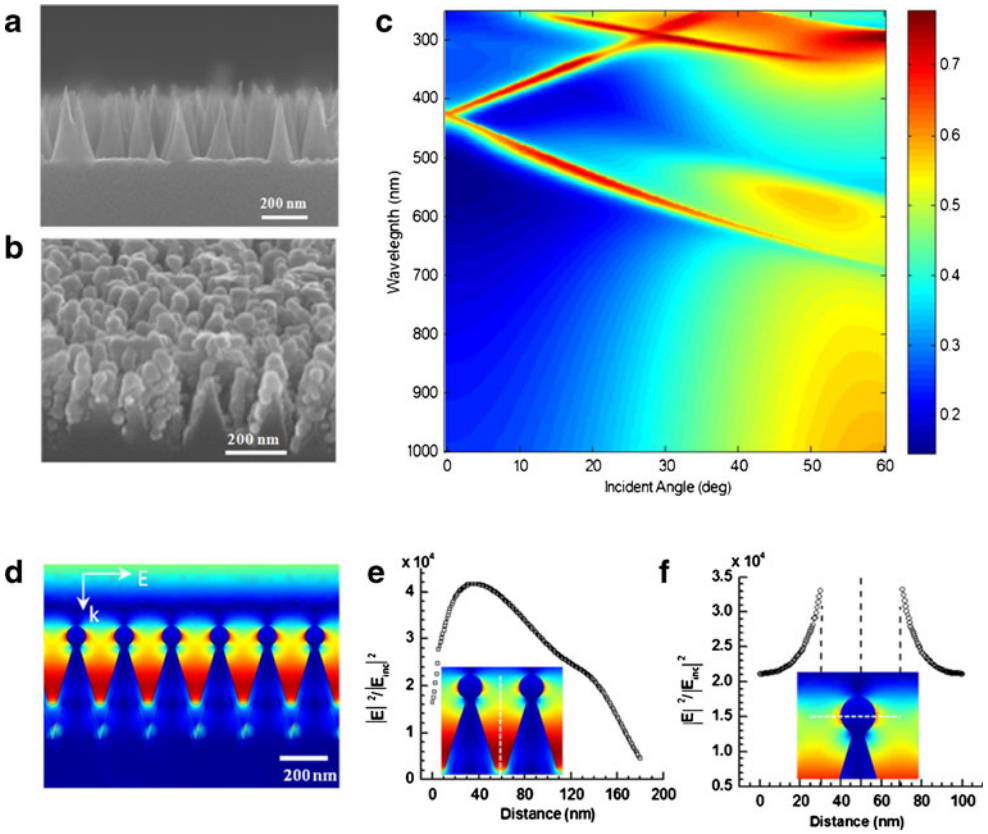

Fig. 3 **a** SEM image of the nanocone silicon based photonic structure. **b** SEM image of the nanoplasmonic structure fabricated from the nanophotonic structure shown in **a** by depositing 80 nm of silver using electron beam evaporation. **c** Dispersion diagram of the nanoplasmonic structure shown in **b** using RCWA method. **d** Calculated electromagnetic field for the nanoplasmonic structure. **e** Gap mode surface plasmon resonance and the corresponding enhancement of the electromagnetic field calculated using COMSOL. **f** Tip mode localized surface plasmon resonance and the corresponding enhancement of the electromagnetic field at the tip of the plasmonic structure

80 nm. The absorption efficiency (also the reflection efficiency) of the TM resonant mode was calculated in the wavelength range of $200<\lambda<900$ nm and the incident angle was varied from $0°<\theta<60°$. Figure 3c presents the dispersion diagram of the aforementioned nanoplasmonic structure. The dispersion diagram clearly shows that the nanocone plasmonic substrate can support broadband SPR supporting many incident wavelengths in the range 200–

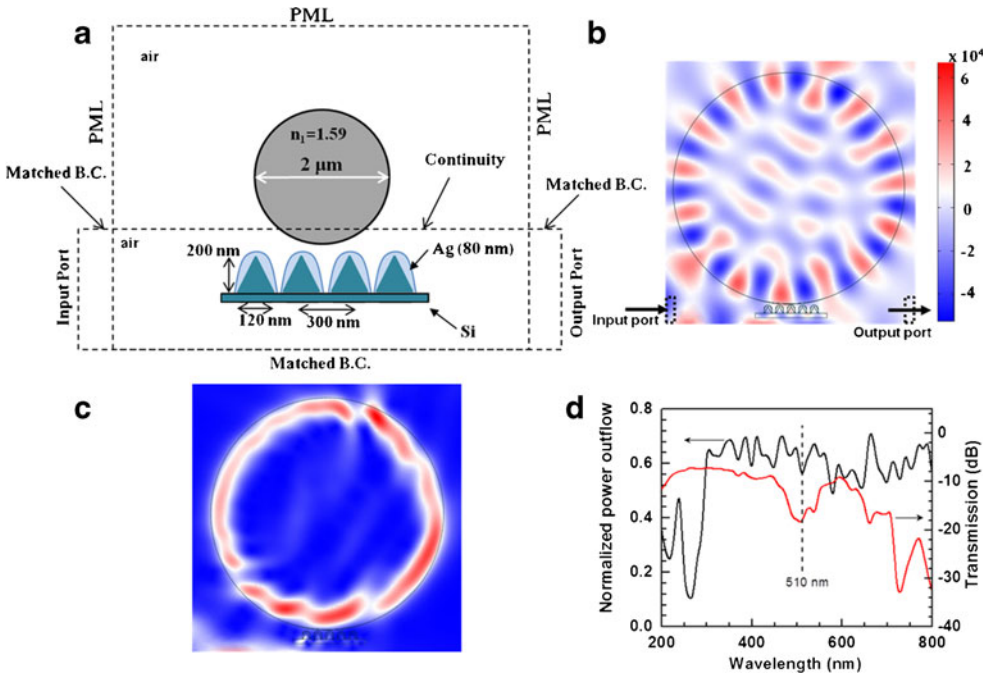

Fig. 4 **a** Schematic with dimensions and boundary conditions for nanocone plasmonic and dielectric microresonator WGM coupling. **b** WGM in a 2 μm silica sphere on a nanocone plasmonic structure. **c** Normal component of Poynting vector at resonance. **d** Normalized power outflow and transmittance near WGM

700 nm covering various incident angles from 0° to 60°. The electromagnetic field distribution within the nanocone plasmonic structure is simulated by COMSOL. The complex optical constants of silver and silicon are taken from Palik's handbook [25]. Figure 3d shows the excited scattering field in TM mode for an incident wavelength of 785 nm. The different colors indicate the magnitude of normalized amplitude of scattering electric field with respect to that of incident electric field, red indicating high field, and blue indicating low field [26]. Two different LSPR modes, namely, the "gap" mode (Fig. 3e) and the "tip" mode (Fig. 3f) can be clearly seen in the simulation. The gap mode is due to the confinement of electromagnetic field in close proximity (<30 nm) between two adjacent nanocone plasmonic structures. The field intensity is enhanced maximum up to 4×10^4 times as compared to the incident field intensity $\left(I_{\text{inc}} = |E_{\text{inc}}|^2\right)$. The high electromagnetic field at the top of cone structure is due to LSPR at the sub 20 nm silver nanobead structures, similar to LSPR observed for metallic naoparticles [27]. The exponential decaying nature of the surface plasmon near-field away from the metal surface can be clearly seen in Fig. 3f.

After confirming that the nanocone structure can support multiple plasmonic modes, we investigate the possibility of coupling the evanescent surface plasmon field in to a dielectric microresonator. The WGM resonance inside the sphere due to SP mode from the nanoplasmonic structure is calculated using a two-dimensional COMSOL simulation. In the present calculations, we launch an in-plane TE waves (as schematically shown in Fig. 4a as input port), where the electric field vector has only a z component and it propagates in the x–y plane. The corresponding dimensions (same as the cone structures described in Fig. 3a, b) and boundary conditions are also shown in Fig. 4a. Figure 4b shows the

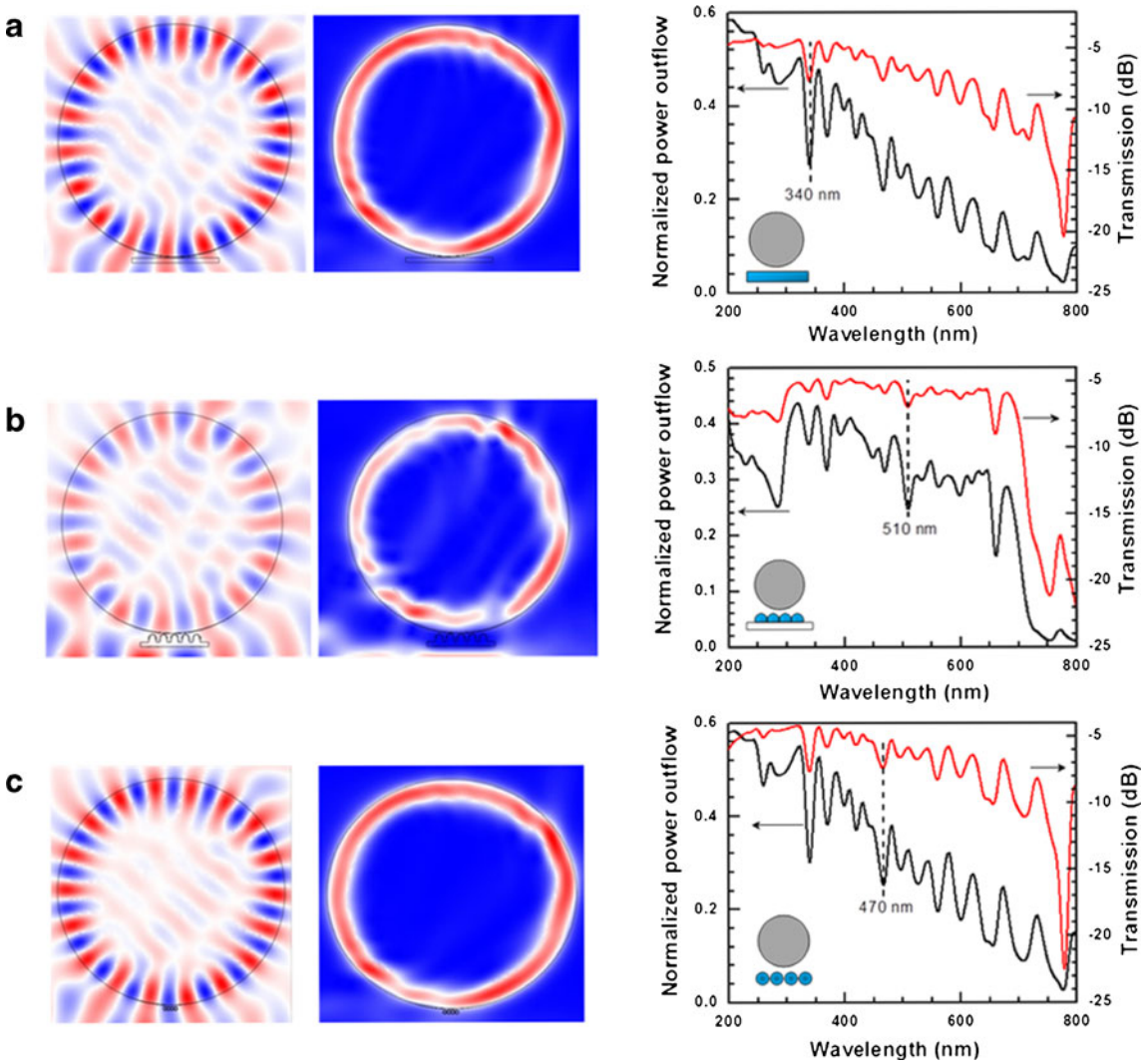

Fig. 5 **a** WGM due to surface plasmon coupling from smooth silver surface to a 2 μm silica sphere. **b** WGM due to surface plasmon coupling from hemispherical silver surface to the silica sphere. **c** WGM due to surface plasmon coupling from periodic array of silver particle to the silica sphere

azimuthal (z-component) electric field at resonance wavelength 540 nm describing WG (n=1, m=15) mode. The corresponding movie is given in the supplementary materials (Movie M1). Interestingly, the prediction of the simple modal analysis which showed that WG resonance occurs near 540 nm, shown in Fig. 2d, matches quite well for nanoplasmonic coupling system shown in Fig. 4b. Figure 4c describes the normal component of Poynting vector at resonance showing the light confinement for the WGM mode. The normalized power outflow collected at the output port is shown in Fig. 4d. The corresponding transmittance is also sketched in Fig. 4d. The resonance is generally characterized by a sharp dip in the transmittance spectra at the resonant coupled mode wavelength. It can be seen that not all scattered power is eventually coupled to the WG mode. There exist only certain wavelengths at which the scattered power is coupled in to the microresonator above it causing a sharp dip in the transmittance spectra at resonance.

Further, we have demonstrated the possibility of SP mode coupling to dielectric WGM mode by simulating several structures supporting both propagating surface plasmon and localized surface plasmon (LSP). Figure 5a simulates WG mode of the dielectric microresonator on the top of a 40 nm thick smooth silver surface. The bulk plasmon for the silver can be excited at around 370 nm (see supplementary Fig. S1) [28]. Figure 5a shows the (n=1, m=18) WG mode of the 2 μm diameter dielectric microresonator due to coupling of surface plasmon field at 340 nm. Figure 5a (middle) also shows the normal component of Poynting vector at resonance. The corresponding normalized power outflow and transmittance near WGM is also plotted in Fig. 5a (right).We have also simulated SP coupling from hemispherical continuous metal surface with silver metal thickness of 100 nm and periodicity of 20 nm (Fig. 5b). The structure can be readily fabricated by nanosphere lithography techniques [29]. The structure showed an SP-coupled (n=1, m=15) WG mode at 510 nm. The corresponding normal component of Poynting vector at resonance, normalized power outflow and transmittance near WGM are also plotted in Fig. 5b. It is well known that nanoparticles can support strong LSPR. Further, the electromagnetic field can be greatly enhanced if "nanogap" can be formed between two adjacent nanoparticles [30]. Here, we simulate the LSPR coupling from four silver nanoparticles with diameter of 30 nm and arranged on the surface so as to make a gap of 2 nm in between them. The high electromagnetic field due to LSPR on the metal nanoparticle surface and in between the gap can be coupled to the dielectric microresonator on top of the particles. Figure 5c shows the (n=1, m=18) WG mode for the microresonator at a wavelength of 470 nm. The normal component of Poynting vector clearly showed the light confinement achieved at resonance. The corresponding normalized power outflow and transmittance near WGM are

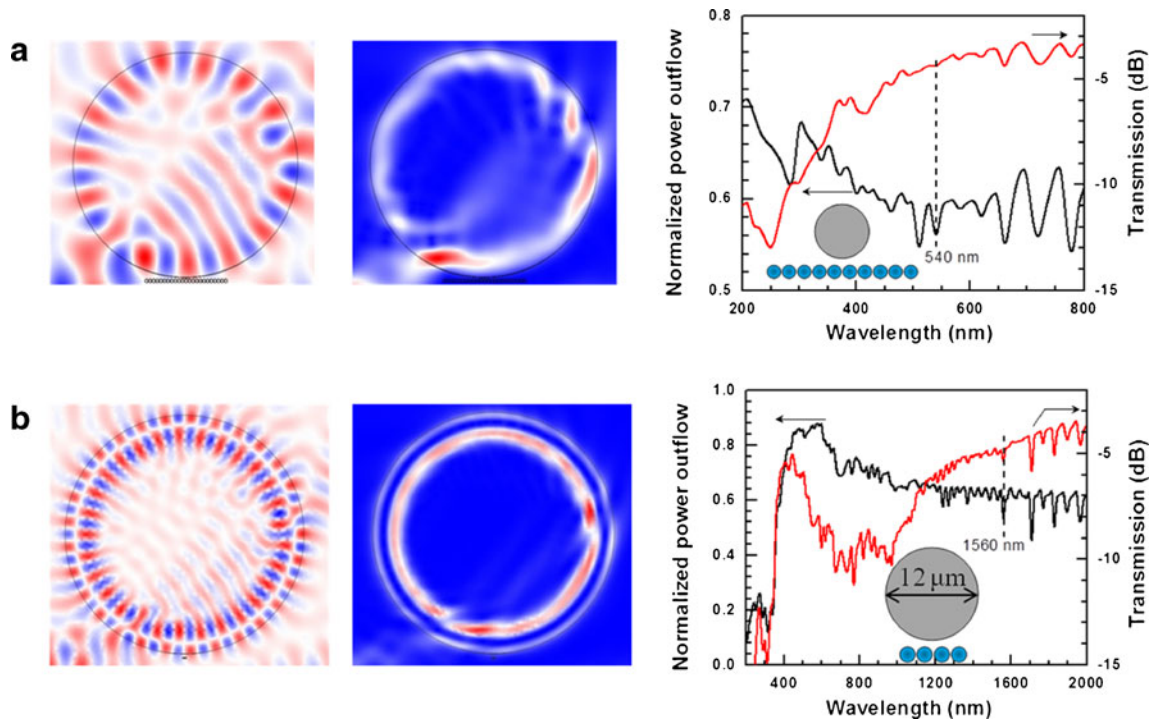

Fig. 6 **a** Effect of increasing the number of plasmonic particles on WG coupling. **b** Effect of increasing the size of the microresonator on surface plasmon coupled WG mode

also shown in Fig. 5c. We observed a red shift of the resonance wavelength for (n=1, m=18) WG mode for smooth silver surface at 340 nm to periodic plasmonic silver particles at 470 nm. We believe that due to higher scattering efficiency even lower energy light can be coupled to the WG mode of the microresonator. This is also evident from the (n=1, m=15) WG mode for nanocone plasmonic structure occurring at 510 nm, which is at lower energy than resonance energy required for smooth silver or plasmonic silver particles.

Figure 6a simulates the effect of increasing the number of plasmonic particles. The size and the gap of the particles were kept constant (30 nm diameter and gap of 2 nm). Total number of particles used for simulation was 23 (earlier we used four particles). With increasing the particle numbers, the mode number shifted from (n=1, m=18) to (n=1, m=15). The resonance wavelength also red-shifted from 470 to 540 nm. This may be due to the fact that periodic array of metal nanoparticles can transport the electromagnetic energy generated due to optical excitation of localized surface plasmon [31]. Hence, with periodic metallic nanoparticles, there exist a possibility of coupling both high energy LSPR and low energy propagating SPR in to the WG modes. We also investigate the effect of increasing the size of the dielectric sphere keeping the number, size and gap of plasmonic particles same as in Fig. 5c. With increasing size (from 2 to 12 μm), we observed a second-order radial mode (n=2, m=29) WG at 1.56 μm (Fig. 6b).

Conclusion

In summary, we demonstrate the surface plasmon coupling to WGM with the assistance of surface plasmon wave on nanoplasmonic structures generated by free-space electromagnetic field. The differences in coupling into TE WG modes with various nanoplasmonic structures are discussed which may lead to different design criteria of plasmonic nanostructures.

References

1. Vahala KJ (2003) Optical microcavities. Nature 424(6950):839–846
2. Vollmer F, Arnold S (2008) Whispering-gallery-mode biosensing: label-free detection down to single molecules. Nat Methods 5 (7):591–596
3. Sandoghdar V, Treussart F, Hare J et al (1996) Very low threshold whispering-gallery-mode microsphere laser. Phys Rev A 54(3): R1777–R1780
4. Braginsky VB, Gorodetsky ML, Ilchenko VS (1989) Quality-factor and nonlinear properties of optical whispering-gallery modes. Phys Lett A 137(7–8):393–397
5. Spillane SM, Kippenberg TJ, Vahala KJ (2002) Ultralow-threshold Raman laser using a spherical dielectric microcavity. Nature 415 (6872):621–623
6. Michler P, Kiraz A, Becher C et al (2000) A quantum dot single-photon turnstile device. Science 290(5500):2282
7. McKeever J, Boca A, Boozer AD et al (2004) Deterministic generation of single photons from one atom trapped in a cavity. Science 303(5666):1992–1994
8. Hijlkema M, Weber B, Specht HP et al (2007) A single-photon server with just one atom. Nat Phys 3(4):253–255
9. Wilk T, Webster SC, Kuhn A et al (2007) Single-atom single-photon quantum interface. Science 317(5837):488–490
10. Cole RM, Sugawara Y, Baumberg JJ et al (2006) Easily coupled whispering gallery plasmons in dielectric nanospheres embedded in gold films. Phys Rev Lett 97(13):137401
11. Little BE, Laine JP, Haus HA (1999) Analytic theory of coupling from tapered fibers and half-blocks into microsphere resonators. J Lightwave Technol 17(4):704–715
12. Shopova SI, Blackledge CW, Rosenberger AT (2008) Enhanced evanescent coupling to whispering-gallery modes due to gold nanorods grown on the microresonator surface. Appl Phys B-Lasers and Optics 93(1):183–187
13. Boriskina SV, Reinhard BM (2011) Spectrally and spatially configurable superlenses for optoplasmonic nanocircuits. Pro Natl Acad Sci USA 108(8):3147–3151
14. Hamam RE, Karalis A, Joannopoulos JD et al (2007) Coupled-mode theory for general free-space resonant scattering of waves. Phys Rev A 75(5):053801
15. Yariv A (1973) Coupled-mode theory for guided-wave optics. IEEE J Quant Electron 9(9):919–933
16. Oraevsky AN (2002) Whispering-gallery waves. Quant Electron 32(5):377–400
17. Lukosz W (1991) Principles and sensitivities of integrated optical and surface-plasmon sensors for direct affinity sensing and immunosensing. Biosens Bioelectron 6(3):215–225
18. Weisser M, Menges B, Mittler-Neher S (1999) Refractive index and thickness determination of monolayers by multi mode waveguide coupled surface plasmons. Sensors and Actuators B-Chemical 56(3):189–197
19. Willets KA, Van Duyne RP (2007) Localized surface plasmon resonance spectroscopy and sensing. Annu Rev Phys Chem 58:267–297
20. Ghaemi HF, Thio T, Grupp DE et al (1998) Surface plasmons enhance optical transmission through subwavelength holes. Phys Rev B 58(11):6779–6782
21. Pang S, Beckham RE, Meissner KE (2008) Quantum dot-embedded microspheres for remote refractive index sensing. Appl Phys Lett 92(22):221108
22. Hooper IR, Sambles JR (2002) Dispersion of surface plasmon polaritons on short-pitch metal gratings. Phys Rev B 65(16):165432
23. Gartia MR, Chen Y, Liu GL (2011) Photoluminescence and cathodoluminescence from nanostructured silicon surface. Appl Phys Lett 99(15):151902
24. Chen Y, Xu Z, Gartia MR et al (2011) Ultrahigh throughput silicon nanomanufacturing by simultaneous reactive ion synthesis and etching. ACS Nano 5(10):8002–8012
25. Palik E (1997) Handbook of optical constants of solids. Academic, Burlington, MA, USA
26. Xu Z, Chen Y, Gartia MR et al (2011) Surface plasmon enhanced broadband spectrophotometry on black silver substrates. Appl Phys Lett 98(24):241904
27. Murray WA, Barnes WL (2007) Plasmonic materials. Adv Mater 19(22):3771–3782

28. Gartia MR, Hsiao A, Sivaguru M et al (2011) Enhanced 3D fluorescence live cell imaging on nanoplasmonic substrate. Nanotechnology 22(36):365203
29. Hulteen JC, Vanduyne RP (1995) Nanosphere lithography—a materials general fabrication process for periodic particle array surfaces. J Vac Sci and Tech 13(3):1553–1558. A-Vacuum Surfaces and Films
30. Chen T, Wang H, Chen G et al (2010) Hotspot-induced transformation of surface-enhanced Raman scattering fingerprints. ACS Nano 4(6):3087–3094
31. Maier SA, Kik PG, Atwater HA et al (2003) Local detection of electromagnetic energy transport below the diffraction limit in metal nanoparticle plasmon waveguides. Nat Mater 2(4):229–232